19th International Symposium on the Application of Laser and Imaging Techniques to Fluid Mechanics · LISBON | PORTUGAL · JULY 16 – 19, 2018

SAND2018-5245C

3D Particle Location from Perspective-Shifted Plenoptic Images

Elise Munz Hall[1,2], Daniel R. Guildenbecher[2], Brian S. Thurow[1,*]

1: Department of Aerospace Engineering, Auburn University, United States

2: Sandia National Laboratories, United States

* Correspondent author: thurow@auburn.edu

Keywords: Plenoptic, particle tracking, light field imaging

HIGHLIGHTS

- 3D particle location measurements from perspective shifted plenoptic images and Direct Light Field Calibration Method
- Improved uncertainty as compared to previous analysis of depth from focus implementation
- Achieves average depth location measurement precision of approximately 0.2 mm over a range of 50 mm
- Computational time requirement reduced by two orders of magnitude as compared to depth from focus implementation

ABSTRACT

3D particle location methods have previously been developed using the refocusing capabilities of plenoptic imaging due to the straightforward nature of refocused images as a volumetric representation of a particle field. This work develops an algorithm to determine 3D particle position by exploiting the perspective-shift capabilities of the plenoptic camera and application of the Direct Light Field Calibration method. This algorithm is validated using an experimental data set previously examined in a refocusing based particle location study in which a static particle field is translated known distances. This data set includes measurements with varied magnification and object distance. Preliminary results suggest increased accuracy and precision can be achieved using the newly developed algorithm at significantly reduced computational costs. The new algorithm also allows the measurement of particles at large distances from the nominal focal plane that previously were unmeasurable due to depth of field limitations of computational refocusing.

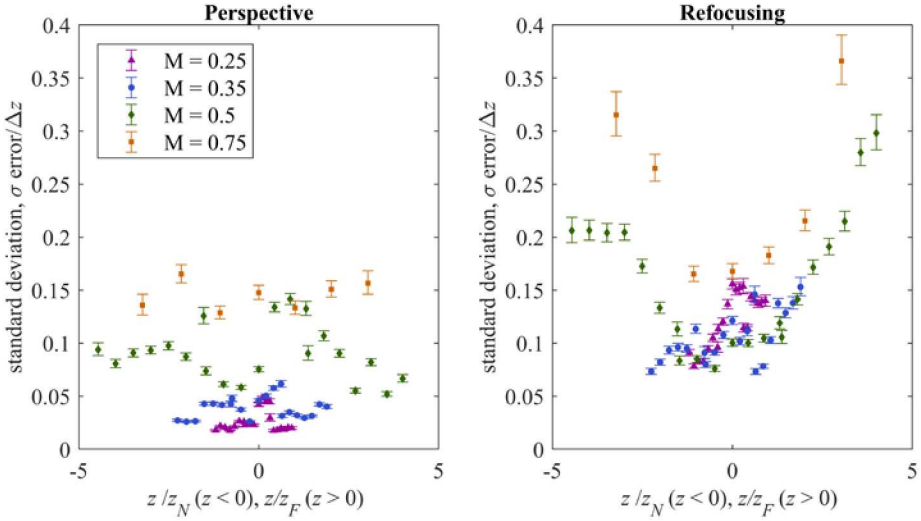

Fig. 1 Standard deviation of depth error (normalized by theoretical depth resolution) as a function of particle depth, z (normalized by depth of field) using (a) perspective shift and (b) refocusing based depth measurement.

3D Particle Location from Perspective-Shifted Plenoptic Images

Elise Munz Hall[1,2], Daniel R. Guildenbecher[2], Brian S. Thurow[1,*]
1: Department of Aerospace Engineering, Auburn University, United States
2: Sandia National Laboratories, United States
* Correspondent author: thurow@auburn.edu

Keywords: Plenoptic, particle tracking, light field imaging

ABSTRACT

3D particle location methods have previously been developed using the refocusing capabilities of plenoptic imaging due to the straightforward nature of refocused images as a volumetric representation of a particle field. This work develops an algorithm to determine 3D particle position by exploiting the perspective-shift capabilities of the plenoptic camera and application of the Direct Light Field Calibration method with a focus on determining not only particle location but also size and shape. This algorithm is validated using an experimental data set previously examined in a refocusing based particle location study in which a static particle field is translated known distances. This data set includes measurements with varied magnification and object distance. Preliminary results suggest increased accuracy and precision can be achieved using the newly developed algorithm at significantly reduced computational costs. The new algorithm also allows the measurement of particles at large distances from the nominal focal plane that previously were unmeasurable due to depth of field limitations of computational refocusing.

---

1. Introduction

Plenoptic imaging is an implementation of light field imaging in which spatial multiplexing by means of a microlens array is used to encode a 4D light field onto a 2D sensor plane, thus capturing both the spatial and angular information defining the light rays emanating from a scene. This allows for the creation of a 3D representation of a scene from a single snapshot. Though this concept originated over a century ago, described as integral photography (Lippmann, 1908), practical implementations of plenoptic cameras are a more recent development linked to the availability of high resolution digital image sensors and computational capability increases. Adelson and Wang presented the first implementation of a plenoptic camera in 1992 (Adelson & Wang, 1992), and Ng. et al created a handheld version in 2005 (Ng, Levoy, Duval, Horowitz, & Hanrahan, 2005). Since these early implementations, the development and use of this technology has greatly increased. Plenoptic cameras have been applied to a wide variety of scientific applications including many implementations of volumetric particle based imaging techniques (Chen & Sick, 2017; Chen, Sick, Woodward, & Burke, 2017; Fahringer, Lynch, & Thurow, 2015;

Hall, Thurow, & Guildenbecher, 2016; Johnson, Thurow, Kim, Blois, & Christiansen, 2017; Truscott, Belden, Ni, Pendlebury, & McEwen, 2017). The current work is specifically motivated by the need for 3D diagnostics of explosively generated fragments.

Previously, the refocusing capability of plenoptic imaging has been exploited to determine particle positions from a series of computationally refocused images and metrics of uncertainty and computational efficiency have been obtained (Hall, Guildenbecher, & Thurow, 2017). The use of refocused images to obtain particle locations is perhaps the most obvious use of plenoptic data for particle location; however, plenoptic data can also be used to create perspective-shifted images. In this work, an algorithm is developed to exploit the perspective-shift capability of plenoptic imaging to determine 3D particle positions. This algorithm is applied to the same data set used in (Hall, Guildenbecher, et al., 2017) to compare the uncertainty characteristics and efficiency of this algorithm to the previously implemented refocusing based technique.

2. Background and previous work

The plenoptic camera implementation discussed in this work uses a standard scientific camera that is modified by the insertion of a microlens array placed between the main lens and the image sensor. These microlenses redirect incoming light rays to different image sensor locations according to angle of propagation, resulting in an instantaneous image that contains volumetric information. Each microlens creates a sub-aperture image of the main lens aperture as shown in Fig. 1 where a raw plenoptic image of an array of pinheads used to represent a particle field is shown on the left. Straight pins are used to represent static particles to allow for uncertainty analysis. The following inset images demonstrate the sub-aperture images that simultaneously encode spatial and angular information. For convenience, a two-plane parameterization is used to fully define the light ray locations in space where (u,v) defines coordinates on the main lens aperture and (s,t) defines coordinates on the microlens plane, again shown in Fig. 1. The light field, which defines the amount of light travelling in all directions through all points in space, is a function of these four coordinates, $L(u,v,s,t)$. In post-processing this additional information can be used to create volumetric representations of the scene by computationally changing the depth of the focal plane or the angle from which the scene is viewed. These are termed refocused and perspective-view images respectively and each contain information that can be used to identify particle position in 3D space.

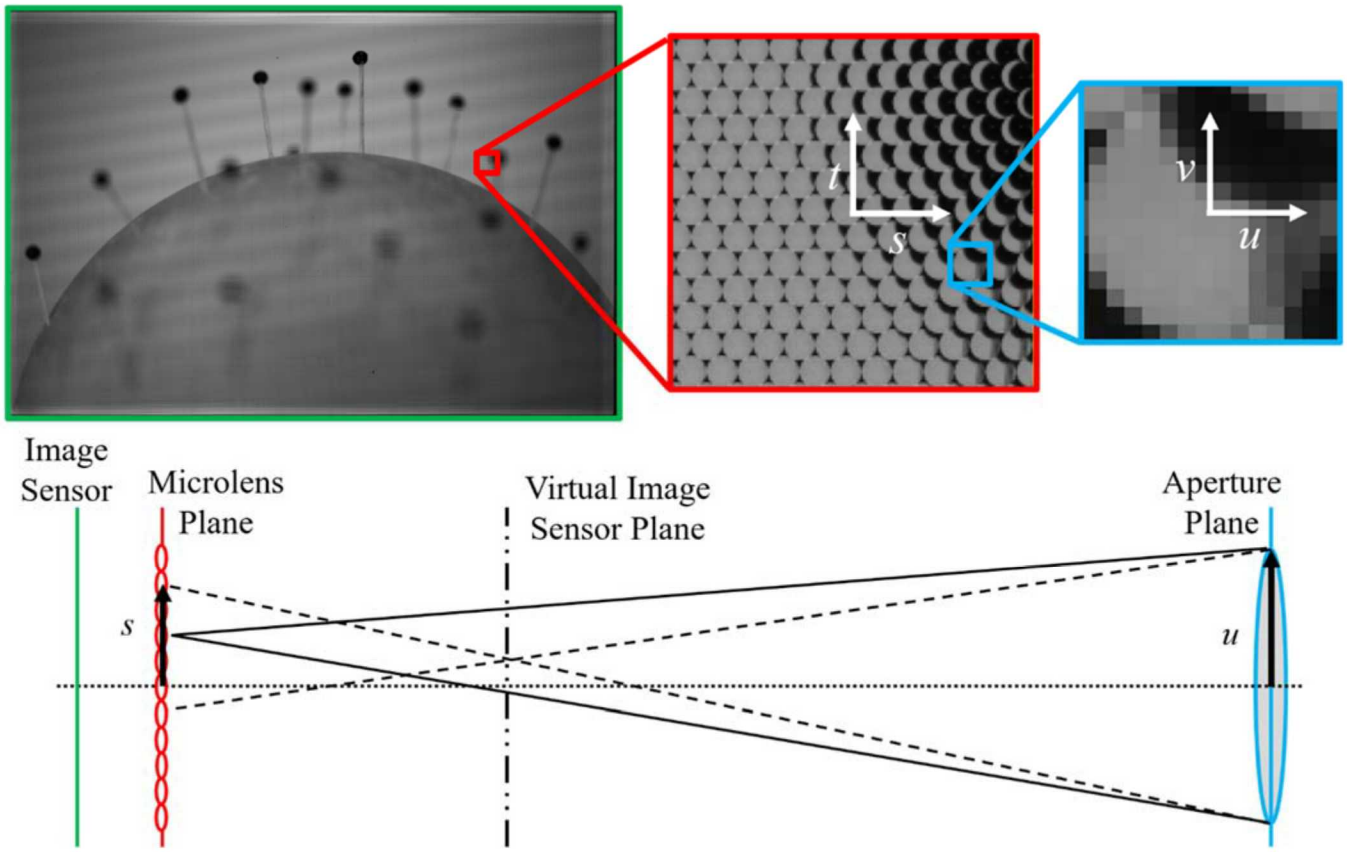

Fig. 1 Raw image and insets corresponding to the two-plane parameterization (top) and schematic depicting the elements of plenoptic imaging (bottom)(Hall, Guildenbecher, et al., 2017).

A. Refocusing

Computationally changing the depth at which the image is focused is achieved by a shifted integration over the sub-aperture images. Fig. 2 demonstrates an example where the raw image from Fig. 1 is refocused to two different depths, which can be seen in comparing which particles appear in focus in each image. Creating refocused images at a variety of depths in this manner produces a conceptually straightforward method of a volumetric representation of a scene, which is called a focal stack. In previous works (Hall, Fahringer, & Thurow, 2017; Hall, Guildenbecher, et al., 2017; Hall et al., 2016), focal stacks with many slices were used to determine 3D locations of particles using a modified version of the hybrid particle detection method based on minimum intensity and maximum edge sharpness which was originally developed for holography (Guildenbecher, Gao, Reu, & Chen, 2013). Due to the requirements of integration over all pixels behind each microlens and using a sufficient number of depth planes, the creation of these focal stacks is a computationally expensive process.

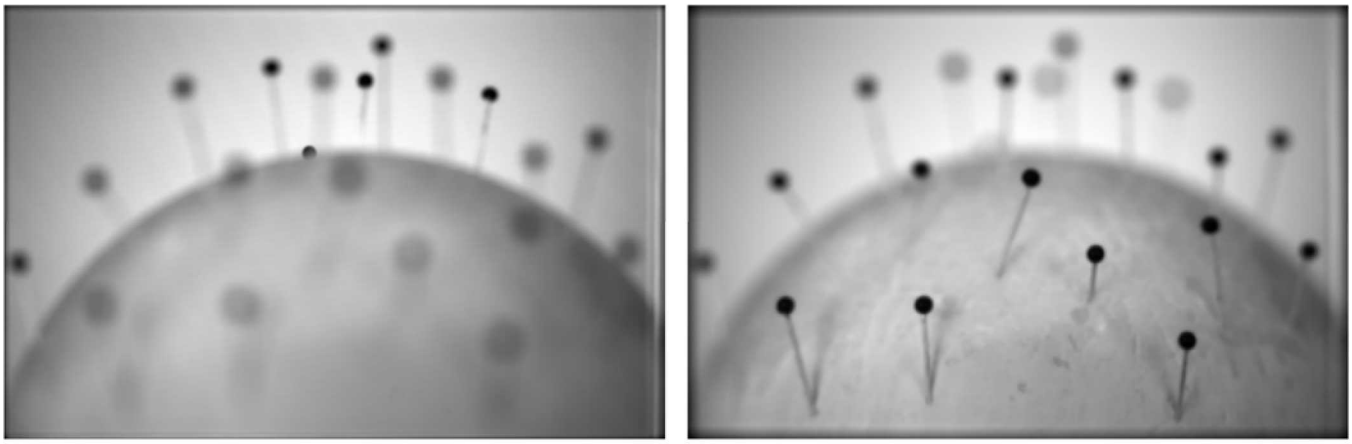

(a) (b)

Fig. 2 Example of refocusing capability, an image focused (a) farther from and (b) nearer to the camera than the nominal focal plane.

B. Perspective-shift

Creating a perspective-shifted image can be described as combining the pixel from behind the same aperture location relative to each microlens and is mathematically defined by,

$$E(s,t) = L(u_0, v_0, s, t), \qquad (1)$$

where (u_0, v_0) is the selected aperture location. As compared to refocusing, the creation of perspective views is mathematically simpler and therefore implementation requires significantly less computational resources. An example of a perspective-shift is shown in Fig. 3 where the raw image from Fig. 1 was shifted to the left and right. The shift is most evident in comparing the relative distance between objects as noted in the colored ovals. The relative location of an object in different perspective-views provides an indication of the location of the objects in 3D space, though in a less obvious manner than in determining depth from focus.

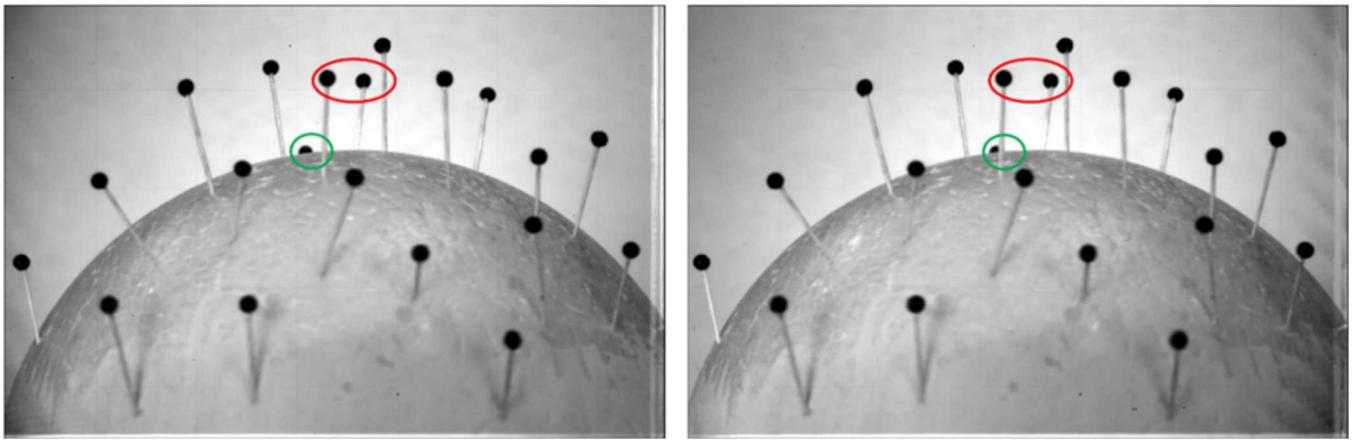

(a) (b)

Fig. 3 Example of perspective-shift capability, an image shifted to the (a) left and (b) right.

3. Particle location algorithm

The algorithm developed in this work uses the apparent discrepancy in 2D particle locations between different perspective views to determine 3D particle locations. This method is conceptually similar to those used in stereo imaging except that many more views are used, which provides redundancy and allows erroneous measurements to be identified and removed without removing an entire particle measurement.

A. Volumetric calibration

To account for lens distortions and other experimental error, the Direct Light Field Calibration (DLFC) is applied in the determination of object space particle locations. Creation of the calibration coefficients required for DLFC is based on a range of dot cards with known physical dimensions as described in (Hall, Fahringer, et al., 2017). Here, a 4th order polynomial fit is used rather than a 3rd order as was done in (Hall, Fahringer, et al., 2017). This increase in order was executed because in application of a 3rd order fit, a distinct systematic warping was still present in the resulting data as indicated by measurement of particle locations in dot card images. Application of a 4th order fit, which required 126 coefficients in each dimension, removed this systematic error. This calibration is created only once for a given experimental condition and results in a modification of the perspective-shift equation where Eq. (1) becomes,

$$E(s,t) = L(u_0, v_0, P_s(X,Y,Z,u,v), P_t(X,Y,Z,u,v)), \qquad (2)$$

where P_s and P_t define the polynomial fit in each dimension. To determine the effect of this increase in polynomial order on previous data processing, a small portion of the data set from previous work (Hall, Guildenbecher, et al., 2017) was reprocessed using the refocusing based method and a 4th order polynomial fit. The resulting measurements showed negligible differences, suggesting that the use of a higher order polynomial is only necessary in measurements using perspective-shifted images.

B. Perspective view particle location

The process of determining particle location begins with the creation of a range of perspective-shifted images from a single raw image using the Light Field Imaging Toolkit (Bolan, Hall, Clifford, & Thurow, 2016). Particle locations are measured in each of these views using standard MATLAB region finding tools, which define particles as connected regions of pixels with intensities below dynamically determined maximum intensity thresholds. The sets of particle images from individual views are then grouped by particle using MATLAB's k-means clustering functionality. This process for a single data image is described in Fig. 4. The use of a clustering

technique allows the comparison of the particle images from all views simultaneously, avoiding issues that arise in matching between pairs of views that may be missing one or more particles or have problematic image artifacts.

The k-means algorithm minimizes the average squared distance between points in the same cluster for a given number of clusters, k (Arthur & Vassilvitskii, 2007). In the current application, these points are the images of a single particle in different perspective views. The selection of initial cluster centroids, or seeds, has a dramatic effect on the results, therefore, strategic selection of these points is critical. To improve the likelihood of minimization, the k-means algorithm is executed for 50 sets of seed points determined by the k++ means algorithm and using only the center 49 perspective views. Then the resulting minimized set of centroid locations is used to initialize a final run of the clustering including a larger range of perspective views (Arthur & Vassilvitskii, 2007). Since k-means clustering depends on an input of the number of expected clusters and the number of particles in each image is not known, the clustering routine is repeated using a range of k values centered on the number of particles most commonly identified in the perspective views. The overall solution that minimizes the average distance between particle images and cluster centroids is selected as the correct solution.

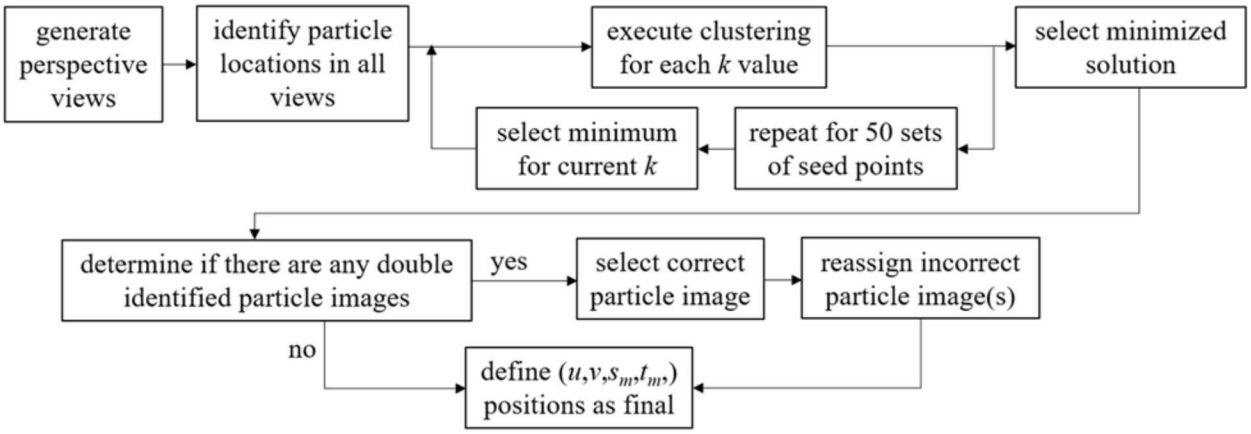

Fig. 4 Flow chart depicting the determination of particle image sorting and (u,v,s,t) measurements.

In the case of overlapping particles, this solution can sometimes result in more than one particle image from a single view being identified as belonging to a single particle (cluster). This is rectified by first determining an expected position for the particle image from that view based on the measured positions of the other views of that particle. Then, the particle image that is closest to the expected location is selected as the correct particle image. Finally, the rejected particle image is reassessed to determine with which particle it should be associated (if more than one particle

image was rejected all are reassessed and reassigned). This results in a list of measured (u,v,s,t) locations for each particle, denoted (u,v,s_m,t_m).

C. 3D particle location

The determination of the (x,y,z) object space location for a single particle is described in Fig. 5. First the (x,y,z) position which minimizes the DLFC relationship defined by the calibration coefficients for the (u,v,s_m,t_m) locations is determined using a MATLAB nonlinear solver. To allow rejection of measurement outliers, the relationship defined by DLFC is used directly to define the calculated (u,v,s,t) locations, (u,v,s_c,t_c), which correspond to the (x,y,z) position. These (u,v,s_c,t_c) locations are compared to the (u,v,s_m,t_m) locations and any measurements which show large discrepancies are discarded and the remaining measurements are used to determine a refined (x,y,z) position. The discrepancy is defined as the magnitude of the distance between the measured and calculated (s,t). This iteration continues until all (s,t) discrepancies are below a prescribed threshold (experimentally any magnitudes larger than three standard deviations from the median). In this way, a small number of erroneous measurements of the location of a particle can be removed while still allowing a valid determination of the position of that particle.

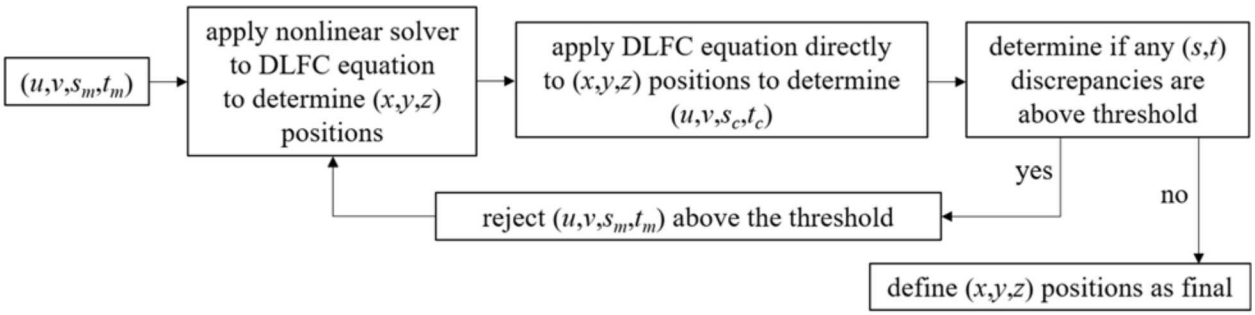

Fig. 5 Flow chart depicting the determination of (x,y,z) object space locations from (u,v,s,t) measurements.

4. Results

A. Experimental configuration

The accuracy and precision of particle location measurements achievable using the method developed in this work is assessed using the experimental data set examined in previous work (Hall, Guildenbecher, et al., 2017), in which a rigid particle field is simulated by straight pin heads inserted at random orientations into a foam ball as shown in Fig. 6. The particle field is mounted on a translation stage allowing precise displacements along the optical depth direction, z.

Data was collected at four different magnifications and with the camera positioned at three different distances from the particle field resulting in 12 configurations to allow examination of trends based on field of view and object distance. In each of these configurations, the particle field was translated in 1 mm increments along the entire 50 mm travel distance of the translation stage and images were captured at each position. This process was repeated 50 times for each configuration to achieve a large statistically significant data set. Depth displacement error is defined by the distance of a particle measurement from a linear fit defined by the particle measurements and the translation stage position. Further experimental details and a detailed description of the error calculation method can be found in previous work examining this data set (Hall, Guildenbecher, et al., 2017).

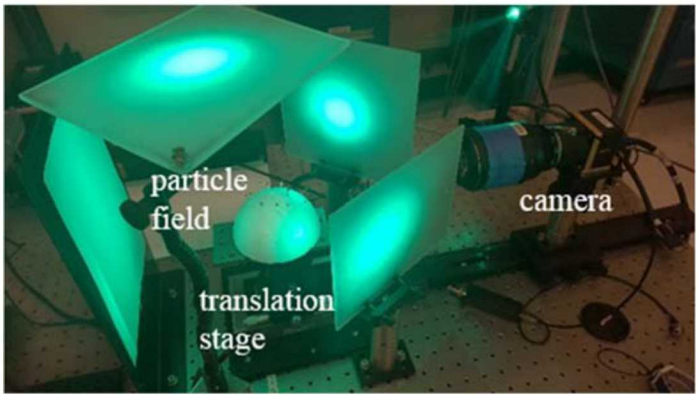

Fig. 6 Experimental configuration including simulated particle field, translation stage, and plenoptic camera.(Hall, Guildenbecher, et al., 2017)

B. Uncertainty analysis

All 12 configurations have been processed using the algorithm developed in this work, providing preliminary indications of the uncertainty achievable using perspective shift based depth determination. Here, accuracy is quantified by average error and precision is quantified by standard deviation of error. All of the error measurements determined from the data set with a magnification of 0.5 and the middle depth configuration are shown in Fig. 7 , which demonstrates that the errors appear to be normally distributed. The number of measurements available and the general scale of errors is also evident from this plot and is similar to those previously obtained using the depth from focus method. This confirms that a valid comparison can be made between the current results and those in (Hall, Guildenbecher, et al., 2017).

Accuracy is considered in Fig. 8, which displays the average depth displacement error as a function of z-location. Vertical error bars show 99% confidence bounds. Fig. 8a displays the results of the perspective shift method while Fig. 8b displays the results from the previous depth from

focus method (Hall, Guildenbecher, et al., 2017). The perspective shift results show not only smaller average errors but in most cases smaller confidence bounds on the measurements demonstrating better consistency of the method.

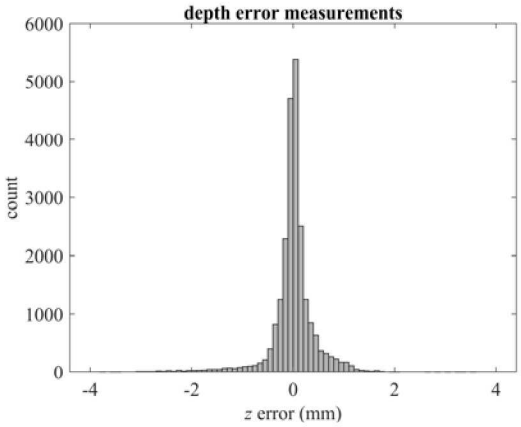

Fig. 7 Histogram of the errors measured from the middle configuration with a magnification of 0.5.

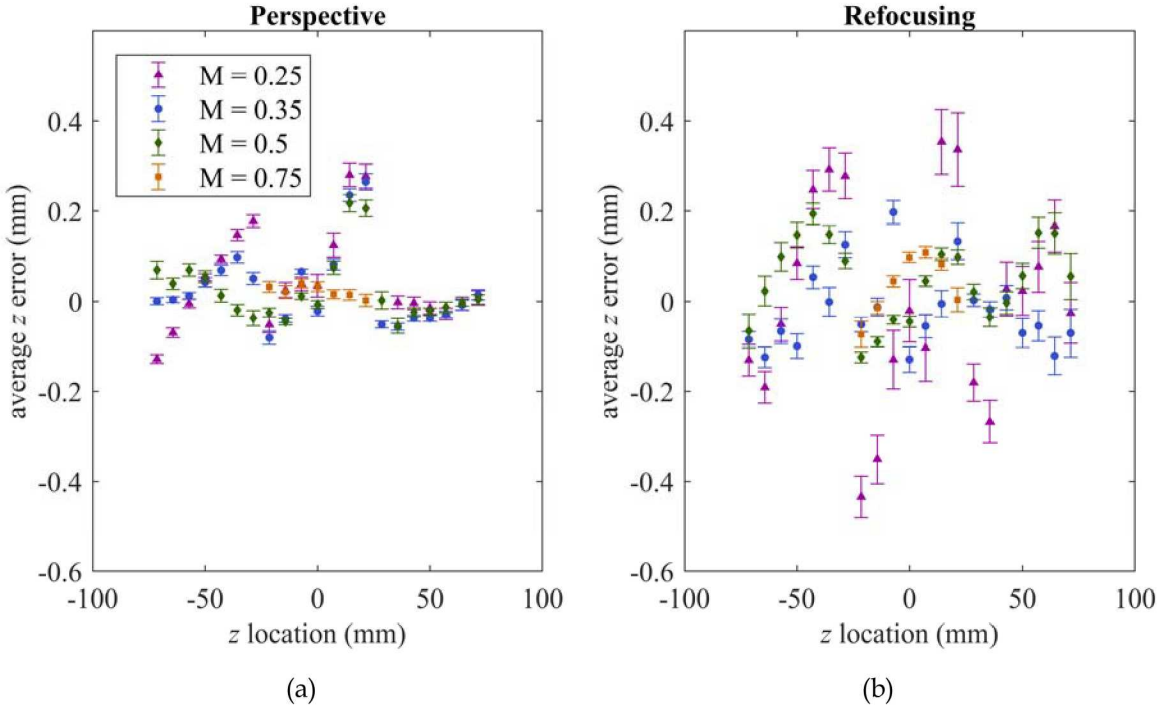

(a) (b)

Fig. 8 Average depth error as a function of particle depth, z, using (a) perspective shift and (b) refocusing based depth measurement.

Fig. 9 displays similar plots of standard deviation, σ, of depth displacement error (as a measure of precision) as a function of z-location. Comparison of these two plots shows that first, the perspective shift method, in general, results in increased precision over the entire range of *z*-

positions. Second, the precision for each magnification remains relatively constant with z in the perspective shift results in contrast to the refocusing based results, which show more variation as a function of depth and of magnification.

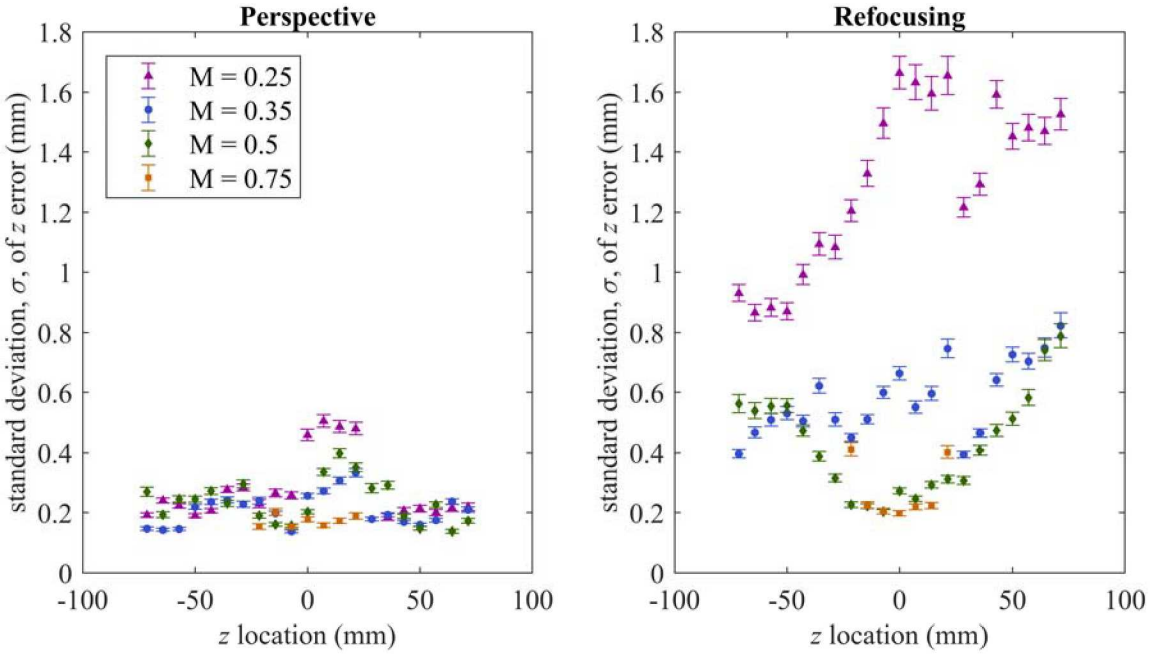

(a) (b)

Fig. 9 Standard deviation of depth error as a function of particle depth, z, using (a) perspective shift and (b) refocusing based depth measurement.

To better understand uncertainty trends as a function of magnification, the theoretical depth resolution, Δz (Deem, Zhang, Cattafesta, Fahringer, & Thurow, 2016), can be compared to these precision measurements. Theoretical depth resolution is a function of physical parameters of the camera and lens as well as the nominal magnification. Table 1 displays the theoretical depth resolution and the measured precision corresponding to a confidence bound of 99.994%, defined by ±4σ, for the perspective and refocusing based methods. The refocusing method showed that this precision measurement roughly corresponded to the theoretical depth resolution, likely because the particle depths were determined from the sharpness of the numerically refocused images. The perspective shift results show not only improved precision but also a less significant change with magnification suggesting that the theoretical depth resolution may not closely bound precision for measurements made using perspective images. Despite this, precision does improve with increasing magnification.

Table 1. Comparison of theoretical and measured depth precision.

	theory	measured precision, ±4 ⌀ (mm)	
M	Δz (mm), Eq. (1)	perspective	refocusing
0.25	10.7	2.5	10.7
0.35	5.4	1.8	4.6
0.5	2.6	2.1	3.5
0.75	1.2	1.4	2.2

Fig. 10 displays normalized versions of the same plots from Fig. 9. The z position is normalized by the near and far limits of the depth of field and the standard deviation is normalized by the theoretical depth resolution, Δz (Deem et al., 2016), for each magnification. These plots show a general loss of normalized precision with increasing magnification using either method. In the refocusing results shown in Fig. 10b, a decrease in precision with increasing distance from the focal plane is evident while the perspective shift results in Fig. 10a show relative consistency as a function of depth. This is indicative of the requirements of each processing method. Depth from focus requires a particle be brought into focus at the depth where it is located, which is not possible at locations far outside the nominal depth of field of the lens configuration. Determination of depth from perspective shift only requires comparison of the locations of a particle in each perspective view; therefore, even a significantly out-of-focus particle can be located with good precision.

This difference in methods is further illustrated in examination of the results from the largest magnification (0.75) configurations, shown in Fig. 11. Due to the small depth of field associated with the large magnification, the data sets at the near and far depths could not be processed in the previous depth from focus work. The particles were so far out of focus that reasonable location identifications could not be made from the dot card focal stacks, thus, a calibration could not be executed. Using the perspective shift method these data sets were processed, though the resulting precision measurements show significant degradation as compared to the other data sets. Additionally, fewer particles were successfully identified at the most extreme depths because of algorithmic requirements that limit the particle measurements that can be considered. Requirements include identification of a given particle in a minimum number of perspective views and maximum error allowances in the DLFC minimization solution. This resulted in artificially high precision measurements at extreme depths because only a small number of particles were identified over a relatively narrow solid angle. For this reason, data from depth regions that did not have enough data (defined by the number of identified particles in a particular region

compared to the median number of particles identified) to provide valid precision measurements is not considered in this work.

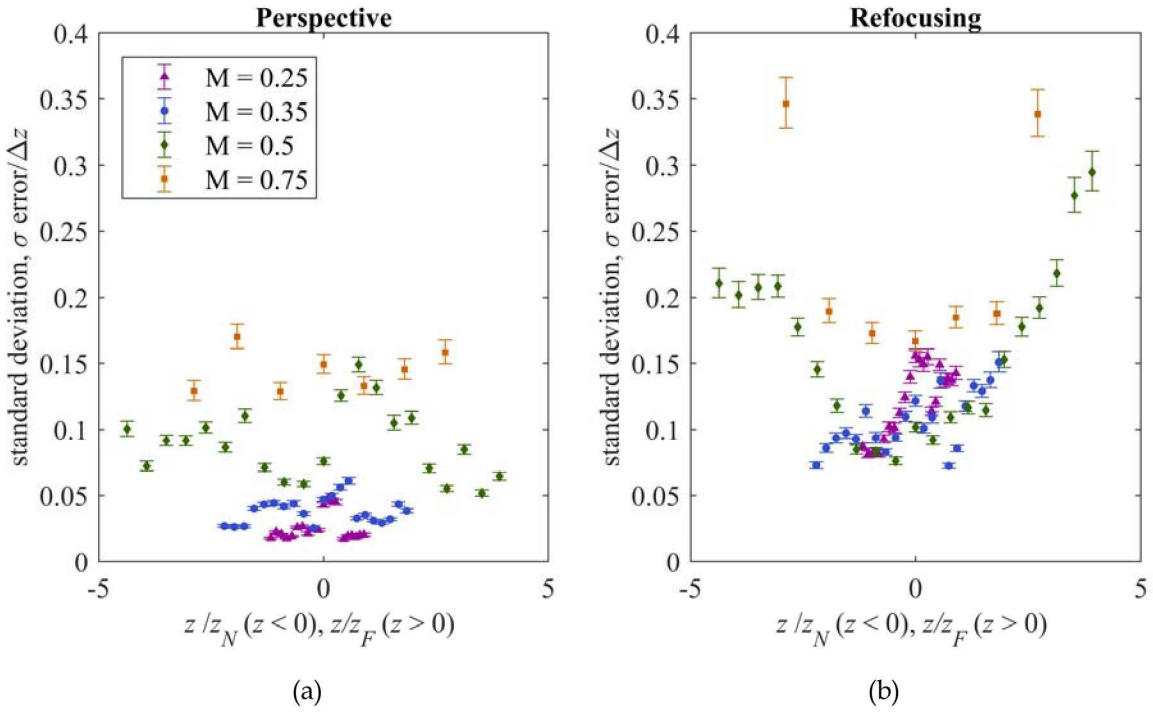

Fig. 10 Standard deviation of depth error (normalized by theoretical depth resolution) as a function of particle depth, z (normalized by depth of field) using (a) perspective shift and (b) refocusing based depth measurement.

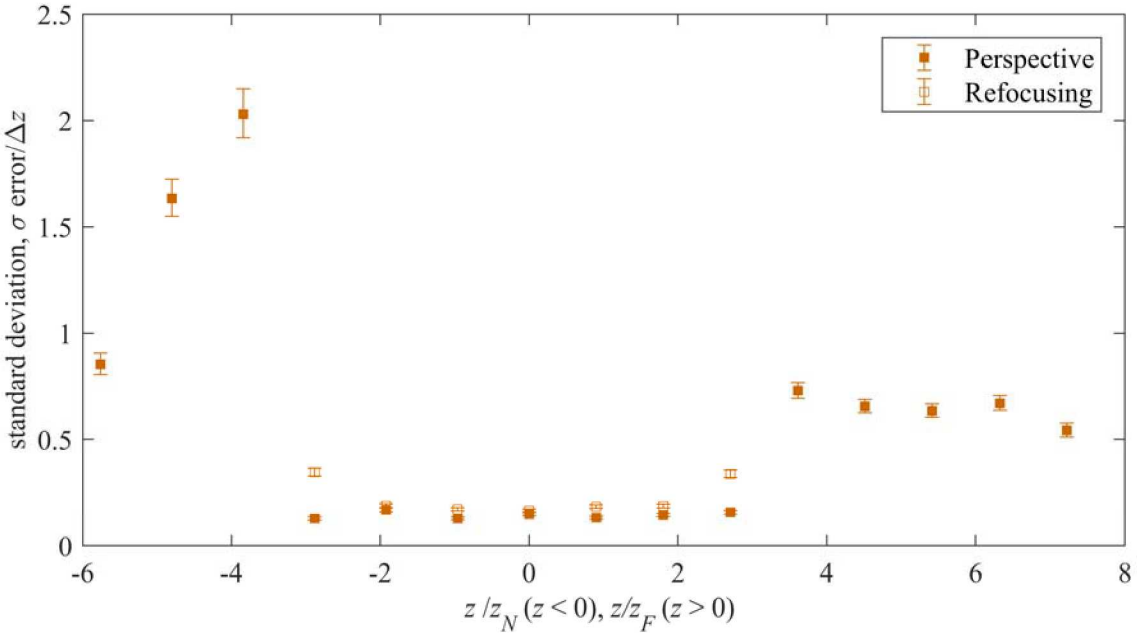

Fig. 11 Standard deviation of depth error as a function of particle depth, z for the largest magnification (0.75). The results of the perspective shift method are shown for all 3 depth configurations, only the center depth configuration is shown using the refocusing based method due to depth of field limitations.

As a qualitative example, dot card images from the largest magnification case are considered. Fig. 12 shows sharpness maps from a small region of two different dot card images depths of z = 0 mm and 75 mm. In each case the sharpness map was created from the refocused image depth with maximum sharpness, however, the results of refocusing to these two depths are dramatically different. Comparison of the two maps shows that the sharpness at the extreme depth of z = 75 mm is approximately two orders of magnitude smaller than at the focal plane and significantly less localized because objects at that depth cannot be brought into focus. Fig. 13 shows a small region of two different perspective views from the same raw dot card image. Though the dots remain out of focus, their relative locations (emphasized by the overlaid black lines) are clearly different. The vertical shift in perspective is evident in examination of the dot positions relative to the black lines.

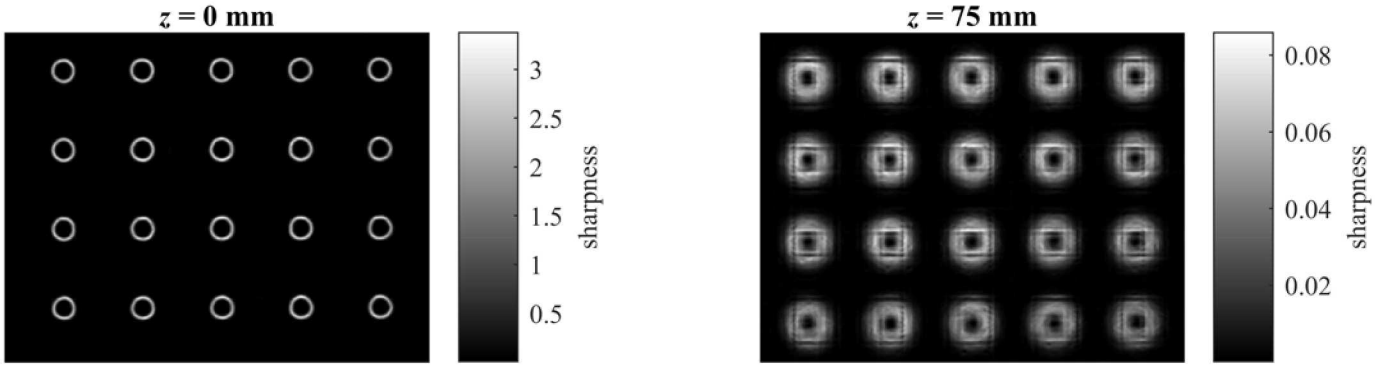

Fig. 12 Sharpness maps of two different refocused dot card images at two different depths, demonstrating the depth ambiguity at large distances from the focal plane.

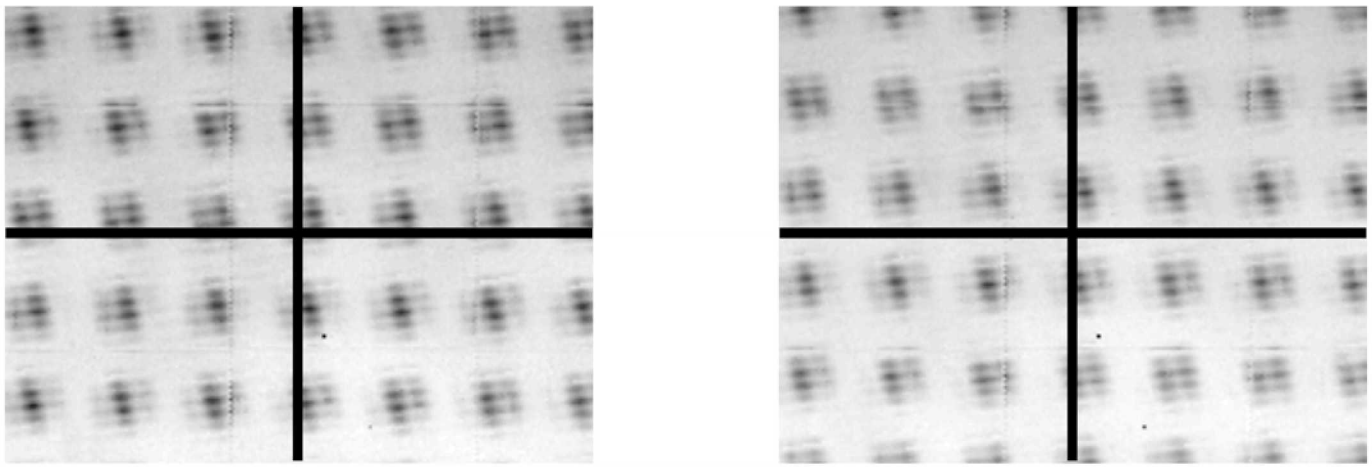

Fig. 13 Perspective views from two different aperture locations, demonstrating that despite an out of focus image, dot location can be identified. Black lines indicate corresponding coordinates in each image for clarity.

C. Computational requirements

The computational requirements of the perspective view algorithm developed here provides a significant advantage over the previous refocusing based method in a reduction of required computational time and resources. All times reported here consider a MATLAB implementation. First, both methods require a preprocessing of the raw image to interpolate the raw hexagonal grid onto a rectilinear grid, which takes approximately 1 minute. The calculation of a focal stack and determination of the particle locations for a single image using the previous method takes approximately 1 hour parallelized on a 12 core desktop computer. The calculation of perspective views and execution of the particle location algorithm described here takes approximately 10 seconds – a decrease of approximately two orders of magnitude. Additionally, the current method has not been parallelized which may allow for further computational reduction. Considering the decreased measurement uncertainties achieved using each method, this speed up is particularly significant. The use of perspective views rather than refocused images also reduces the memory requirement. The refocusing method requires that a large focal stack be stored in RAM, requiring approximately 2 GB of RAM for each image during processing. In contrast, storage of the perspective views requires only 0.2 GB of RAM.

5. Conclusions

This work presents an algorithm developed to measure 3D particle position from perspective-shifted plenoptic images. A range of perspective views is created from a raw plenoptic image and particle image positions are determined in each of these views. These particle images are then sorted by particle using a k-means clustering technique. Finally, the 3D position of each particle is determined by minimizing the relationship defined by the Direct Light Field Calibration coefficients and the positions of all images of that particle.

Application of this method to a particle image data set previously examined using a depth from focus method (Hall, Guildenbecher, et al., 2017) showed improvement in measurement uncertainty and computational efficiency. In this application, average depth location measurement precision of approximately 0.2 mm over a range of 50 mm was achieved. The required computational time was reduced by two orders of magnitude as compared to depth from focus methods.

Further work includes examination of the methods used to identify the particle images corresponding to individual particles to increase the robustness of the particle location algorithm

in the case of more densely seeded particle fields. This includes exploration of the use of only a few views to determine an initial estimate of particle position. This position can be used to reduce the search area in which valid particle images from the remaining views can be located.

Funding

Sandia National Laboratories is a multi-mission laboratory managed and operated by National Technology and Engineering Solutions of Sandia LLC, a wholly owned subsidiary of Honeywell International Inc. for the U.S. Department of Energy's National Nuclear Security Administration under contract DE-NA0003525.

References

Adelson, E. H., & Wang, J. Y. A. (1992). Single lens stereo with a plenoptic camera. *IEEE Transactions on Pattern Analysis and Machine Intelligence*, *14*(2), 99–106. http://doi.org/10.1109/34.121783

Arthur, D., & Vassilvitskii, S. (2007). K-Means++: the Advantages of Careful Seeding. *Proceedings of the Eighteenth Annual ACM-SIAM Symposium on Discrete Algorithms*, *8*, 1027–1025. http://doi.org/10.1145/1283383.1283494

Bolan, J., Hall, E., Clifford, C., & Thurow, B. (2016). Light-Field Imaging Toolkit. *SoftwareX*. http://doi.org/10.1016/j.softx.2016.05.004

Chen, H., & Sick, V. (2017). Three-dimensional three-component air flow visualization in a steady-state engine flow bench using a plenoptic camera. *SAE Int. J. Engines*, *10*, 625–635. http://doi.org/10.4271/2017-01-0614

Chen, H., Sick, V., Woodward, M. A., & Burke, D. (2017). Human iris 3D imaging using a micro-plenoptic camera. *Optics in the Life Sciences*, *2017*, 8–10.

Deem, E. A., Zhang, Y., Cattafesta, L. N., Fahringer, T. W., & Thurow, B. S. (2016). On the resolution of plenoptic PIV. *Meas. Sci. Technol.*, *27*(8), 84003. http://doi.org/10.1088/0957-0233/27/8/084003

Fahringer, T. W., Lynch, K. P., & Thurow, B. S. (2015). Volumetric particle image velocimetry with a single plenoptic camera. *Measurement Science and Technology*, *26*(11), 115201. http://doi.org/10.1088/0957-0233/26/11/115201

Guildenbecher, D. R., Gao, J., Reu, P. L., & Chen, J. (2013). Digital holography simulations and experiments to quantify the accuracy of 3D particle location and 2D sizing using a proposed hybrid method. *Applied Optics*, *52*(16), 3791–3801. http://doi.org/10.1364/AO.52.003790

Hall, E. M., Fahringer, T. W., & Thurow, B. S. (2017). Volumetric calibration of a plenoptic camera. *AIAA SciTech Forum, 55th Annual Aerospace Sciences Meeting*, (January 9-13), 1–13. http://doi.org/10.2514/6.2017-1642

Hall, E. M., Guildenbecher, D. R., & Thurow, B. S. (2017). Uncertainty characterization of particle location from refocused plenoptic images. *Optics Express*, *25*(18), 21801–21814.

Hall, E. M., Thurow, B. S., & Guildenbecher, D. R. (2016). Comparison of three-dimensional particle tracking and sizing using plenoptic imaging and digital in-line holography. *Applied*

Optics, *55*(23), 6410–6420. http://doi.org/10.1364/AO.55.006410

Johnson, K. C., Thurow, B. S., Kim, T., Blois, G., & Christiansen, K. T. (2017). Volumetric velocity measurements in the wake of a hemispherical roughness element. *AIAA Journal*, *55*(7), 2158–2173.

Lippmann, G. (1908). La photographie integrale. *Comptes-Rendus, Academie Des Sciences*, *146*, 446–551.

Ng, R., Levoy, M., Duval, G., Horowitz, M., & Hanrahan, P. (2005). Light field photography with a hand-held plenoptic camera. *Stanford Tech Report CTSR*, 1–11. http://doi.org/10.1.1.163.488

Truscott, T. T., Belden, J., Ni, R., Pendlebury, J., & McEwen, B. (2017). Three-dimensional microscopic light field particle image velocimetry. *Experiments in Fluids*, *58*(3), 16. http://doi.org/10.1007/s00348-016-2297-3